ACES Asian Chemical Editorial Society

DOI: 10.1002/asia.201801588

CHEMISTRY AN ASIAN JOURNAL Full Paper

SPECIAL ISSUE

Aggregation-Induced Delayed Fluorescence Luminogens for Efficient Organic Light-Emitting Diodes

Jiajie Zeng,[a] Jingjing Guo,[a] Hao Liu,[a] Jacky W. Y. Lam,[c] Zujin Zhao,*[a] Shuming Chen,*[b] and Ben Zhong Tang*[a, c]

Abstract: Aggregation-induced delayed fluorescence (AIDF) can be regarded as a special case of aggregation-induced emission (AIE). Luminogens with AIDF can simultaneously emit strongly in solid state and fully utilize the singlet and triplet excitons in organic light-emitting diodes (OLEDs). In this work, two new AIDF luminogens, DMF-BP-DMAC and DPF-BP-DMAC, with an asymmetric D–A–D′ structure, are designed and synthesized. The characteristics of both luminogens are systematically investigated, including single crystal structures, theoretical calculations, photophysical properties and thermal stabilities. Inspired by their AIDF nature, the green-emission non-doped OLEDs based on them are fabricated, which afford good electroluminescence performances, with low turn-on voltages of 2.8 V, high luminance of 52560 cd m^{-2}, high efficiencies of up to 14.4%, 42.3 cd A^{-1} and 30.2 lm W^{-1}, and very small efficiency roll-off. The results strongly indicate the bright future of non-doped OLEDs on the basis of robust AIDF luminogens.

Introduction

With the advantages of low cost, flexibility, self-luminescence and so forth, organic light-emitting diodes (OLEDs) have been considered as one of the most promising techniques for full-color display and solid-state lighting.[1] To date, by reviewing the development of OLEDs, there exists several kinds of light-emitting materials according to their electroluminescence (EL) mechanisms, including fluorescence,[2] phosphorescence,[3] triplet-triplet annihilation (TTA),[4] singlet fission (SF),[5] hybridized local and charge-transfer (HLCT)[6] and thermally activated delayed fluorescence (TADF).[7] Among them, the low-cost purely organic TADF luminogens can theoretically harvest 100% of the electrogenerated singlet (S_1) and triplet (T_1) excitons by rapid reverse intersystem crossing (RISC) owing to their small energy gaps between S_1 and T_1 (usually <0.3 eV).[8,9] However, in most cases, sophisticated doping technique is needed to fabricate OLEDs based on TADF luminogens to avoid some destructive processes,[10] such as aggregation-caused quenching (ACQ), singlet-triplet annihilation (STA),[11] triplet-polaron annihilation (TPA)[12] and TTA.[13]

Creating luminogens with aggregation-induced emission (AIE) property is an ideal way to solve the problem of concentration quenching and simplify the manufacture of OLEDs.[2c,14] Among the AIE luminogens (AIEgens) for the application in OLEDs, silole and tetraphenylethene (TPE) derivatives are very popular, and have been extensively investigated and adopted to make efficient OLEDs with simplified configurations. For example, highly efficient non-doped OLEDs were achieved based on *p*-type TPE derivatives,[14a] which provided high maximum EL efficiencies of 15.7 cd A^{-1}, 12.9 lm W^{-1} and 5.12% for three-layer devices, and 16.2 cd A^{-1}, 14.4 lm W^{-1} and 5.35% for two-layer devices, which is among the best results at that time. However, most of these reported AIEgens are conventional fluorescent molecules, which can merely harvest 25% excitons for light emission. To address this issue, recently, we developed a new variety of luminogens with a charming property of aggregation-induce delayed fluorescence (AIDF).[15] AIDF luminogens are free of ACQ problem and can theoretically utilize 100% of the electrically generated excitons, which have great potential to be applied in non-doped OLEDs.[15,16] To further develop more efficient AIDF luminogens, herein, an asymmetric donor-acceptor-donor′ (D–A–D′) electronic structure composed of a carbonyl acceptor (A) and two different donors (D and D′) is proposed. Although a symmetric D-A-D molecule can also be an AIDF molecule, which takes the advantage of simplicity,[16b] the asymmetric D–A–D′ structure can broaden the diversity of the molecules with delayed fluorescence, which is favored for facilely optimizing their photophysical

[a] J. Zeng, J. Guo, H. Liu, Prof. Z. Zhao, Prof. B. Z. Tang
State Key Laboratory of Luminescent Materials and Devices
Center for Aggregation-Induced Emission
South China University of Technology
Guangzhou 510640 (China)
E-mail: mszjzhao@scut.edu.cn

[b] Dr. S. Chen
Department of Electrical and Electronic Engineering
South University of Science and Technology of China
Shenzhen, Guangdong 518055 (China)
E-mail: chen.sm@sustc.edu.cn

[c] Dr. J. W. Y. Lam, Prof. B. Z. Tang
Department of Chemistry
Hong Kong Branch of Chinese National Engineering Research Center for Tissue Restoration and Reconstruction
The Hong Kong University of Science & Technology
Kowloon, Hong Kong (China)
E-mail: tangbenz@ust.hk

Supporting information and the ORCID identification number(s) for the author(s) of this article can be found under: https://doi.org/10.1002/asia.201801588.

This manuscript is part of a special issue on aggregation-induced emission. Click here to see the Table of Contents of the special issue.

property, carrier transporting ability, electronic structure and so on, by adopting various donor groups in one molecule.[15e] Based on this principle, in this work, the twisted electron-donating 9,9-dimethyl-9,10-dihydro-acridine (DMAC) is used as a donor to form a major D-A structure with electron-accepting carbonyl group, which is responsible for the separation of highest occupied molecular orbital (HOMO) and lowest unoccupied molecular orbital (LUMO), and thus the small ΔE_{ST} for delayed fluorescence. To further depress the intermolecular π–π stacking, two donors of fluorene derivatives with different degrees of steric hindrance, 9,9-dimethylfluorene (DMF) and 9,9-diphenylfluorene (DPF), are employed in the molecular structure. Successfully, the generated new molecules, DMF-BP-DMAC and DPF-BP-DMAC, exhibit prominent AIDF nature and good EL efficiencies in non-doped OLEDs with very small efficiency roll-off.

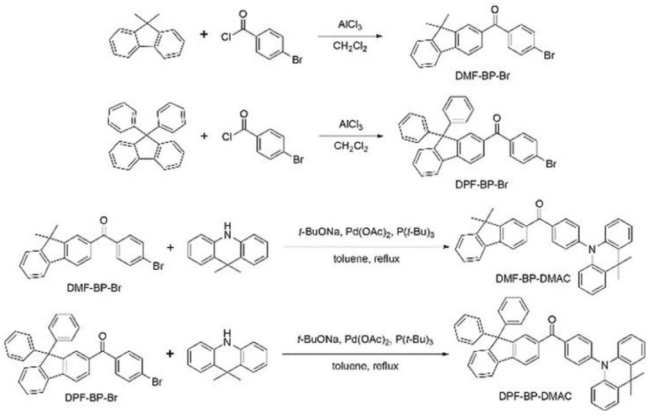

Scheme 1. Synthetic routes and molecular structures of DMF-BP-DMAC and DPF-BP-DMAC.

Results and Discussion

Synthesis

The synthetic routes and molecular structures of DMF-BP-DMAC and DPF-BP-DMAC are depicted in Scheme 1. They are easily synthesized in two steps in high yields via the Friedel–Crafts acylations and Buchwald-Hartwig aminations. Expensive catalysts are not employed in the synthetic routes, so that the total costs of the material synthesis are decreased, which is favored for large-amount production. The final products are further purified by temperature-gradient vacuum sublimation after column chromatography before the measurements of crystal structures, electrochemical properties, photophysical properties, thermal stabilities and EL performances. In addition, DMF-BP-DMAC and DPF-BP-DMAC are highly soluble in widely-used solvents, such as tetrahydrofuran (THF), chloroform, dichloromethane and so forth, but not soluble in water.

Crystal structures

Single crystals of DMF-BP-DMAC and DPF-BP-DMAC are grown from a mixed solution of dichloromethane/*n*-hexane by gradually evaporating the solvents at room temperature and then analyzed by X-ray crystallography. As shown in Figure 1a, both molecules exhibit highly twisted conformations. The torsion angles between DMAC and the adjacent phenyl ring are 82° and 85° for DMF-BP-DMAC and DPF-BP-DMAC, respectively, which conduce to the effective separation of HOMO and LUMO. What's more, the packing patterns of DMF-BP-DMAC and DPF-BP-DMAC are shown in Figure 1c and 1d, respectively. It can be seen that multiple C–H···π and C=O···H hydrogen

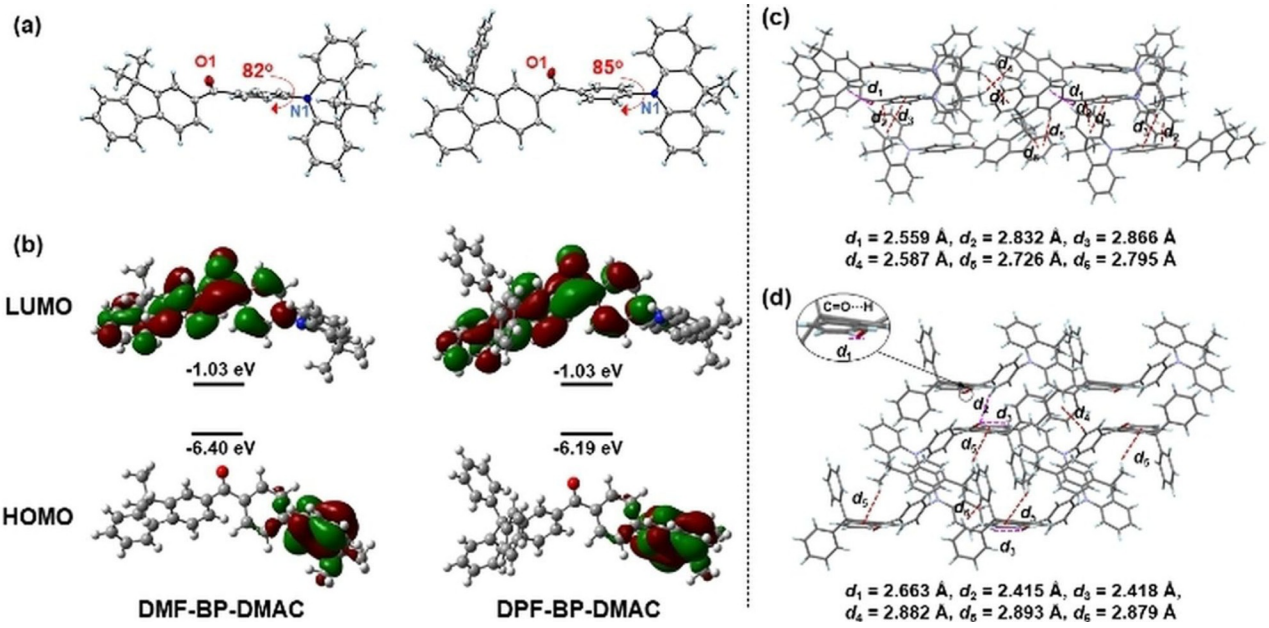

Figure 1. (a) Single crystal structures (CCDC 1572678 and CCDC 1572671 for DMF-BP-DMAC and DPF-BP-DMAC, respectively). (b) Frontier orbital amplitude plots of DMF-BP-DMAC and DPF-BP-DMAC, calculated by the M06-2X hybrid functional at the basis set level of 6-31G(d). Packing patterns of (c) DMF-BP-DMAC and (d) DPF-BP-DMAC in crystals.

bonds are formed amongst molecules, while no π–π stacking can be found due to their twisted conformations. Therefore, nonradiative decay processes in the aggregated state are depressed and, as a result, the luminogens can exhibit strong emission in solid state without emission quenching.

Theoretical calculations

To investigate the electronic structures of both luminogens, quantum-chemical calculations are conducted via density functional theory (DFT) with the M06-2X hybrid functional at the basis set level of 6-31G(d). The optimized structures are obviously twisted as we expected, similar to the single-crystal structures. As shown in Figure 1b, the HOMOs are centered at the DMAC moiety in both luminogens, while the LUMOs are delocalized over the carbonyl core and part of the DMF/DPF units. The HOMOs and LUMOs are essentially separated, ensuring a small ΔE_{ST}. On the other hand, the somewhat overlap between HOMO and LUMO is helpful for achieving both high photoluminescence quantum yields (Φ_{PL}) and delayed fluorescence at the same time.

Photophysical properties

The basic photophysical properties of DMF-BP-DMAC and DPF-BP-DMAC are analyzed by UV-vis absorption, steady photoluminescence (PL) spectra and transient decay PL spectra. As shown in Figure 2a, DMF-BP-DMAC and DPF-BP-DMAC possess similar absorption peaks at ≈320 nm. Extended to ≈430 nm, weak and long absorption tails are observed in both luminogens, which can be ascribed to intramolecular charge transfer (ICT) effect between DMAC and carbonyl groups. In THF solutions, DMF-BP-DMAC and DPF-BP-DMAC exhibit PL peaks at 534 nm and 541 nm with relatively low Φ_{PL} values of 21.9% and 21.7%, while in neat films, DMF-BP-DMAC and DPF-BP-DMAC show strong PL peaks at 509 nm and 515 nm (shown in Figure 2b) with increased Φ_{PL} values of 31.9% and 62.3%, respectively, indicating their AIE properties. Compared to DMF unit, the DPF one is bulkier, which further depresses the π–π interaction in neat film of DPF-BP-DMAC, resulting in a higher Φ_{PL}. Neat films of DMF-BP-DMAC and DPF-BP-DMAC are free of ACQ problem and they are good candidates for non-doped OLEDs.

To further validate the AIE property, the PL behaviors of DMF-BP-DMAC and DPF-BP-DMAC in THF/water mixed systems are then investigated (Figure 2c and 2d). Both luminogens show similar behaviors with the increment of water fraction. The luminogens do not emit strongly until the water fraction (f_w) is increased to 80% and higher. Actually, the PL intensity is decreased as the water fraction increases at first (Figure S1), which is attributed to ICT effect because of the high polarity of water. But as f_w reaches a high value, the aggregates of the luminogens are formed because they are insoluble in water. As a result, the intramolecular motion of the luminogens are restricted, which suppresses the nonradiative process and thus increases PL intensity. Furthermore, owing to the decreased polarity in aggregate,[15e] blue shifted PL peaks are observed when f_w increases.

To dig into the PL mechanisms of both luminogens, the ΔE_{ST} values of their neat films are then obtained from the onsets of fluorescence and phosphorescence spectra at 77 K (Figure S2). Table 1 concludes the key photophysical data of DMF-BP-DMAC and DPF-BP-DMAC. The ΔE_{ST} values of the neat films of DMF-BP-DMAC and DPF-BP-DMAC are measured to be 0.14 eV and 0.09 eV, which are small enough for effective thermally-promoted exciton up-conversion from T_1 to S_1. Therefore, the luminogens are potential emitters with delayed fluorescence. Hence, we measure their transient decay PL spectra at various temperatures in order to verify the potential. Figure 3 shows the temperature-dependent transient decay curves of the luminogens. Roughly, the curves can be split into two segments, a nanosecond-scale prompt decay component and a microsecond-scale delayed component, fitted by the double-exponen-

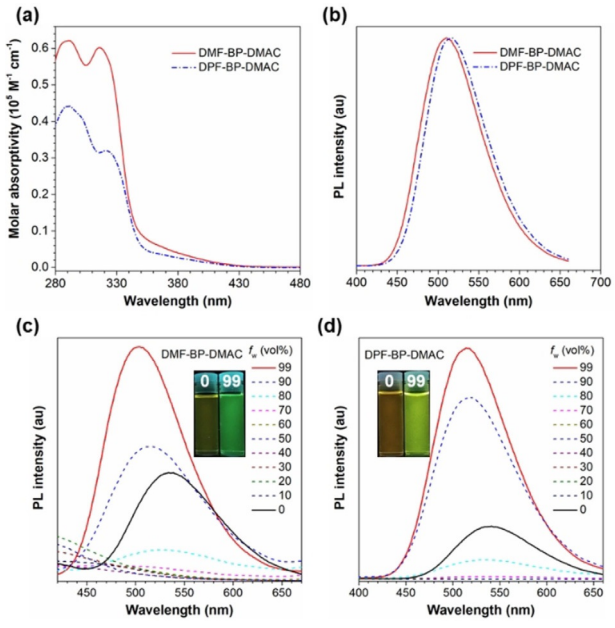

Figure 2. (a) Absorption spectra of DMF-BP-DMAC and DPF-BP-DMAC in THF solution (10^{-5} mol L^{-1}). (b) Normalized PL spectra of the luminogens in neat films. PL spectra of (c) DMF-BP-DMAC and (d) DPF-BP-DMAC in THF/water mixed solutions with various water fraction (f_w); the concentrations of DMF-BP-DMAC and DPF-BP-DMAC are 10^{-5} mol L^{-1}. Inset: photos of DMF-BP-DMAC and DPF-BP-DMAC in THF/water mixtures (f_w = 0 and 99%), taken under a 365 nm UV lamp.

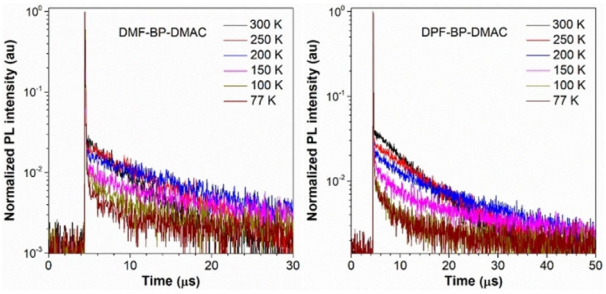

Figure 3. Temperature-dependent transient decay PL spectra of neat films of DMF-BP-DMAC and DPF-BP-DMAC under nitrogen atmosphere.

Table 1. Photophysical data of DMF-BP-DMAC and DPF-BP-DMAC in film.[a]

Emitter	Φ_{PL} [%]	τ_{prompt} [ns]	$\tau_{delayed}$ [μs]	$R_{delayed}$ [%]	Φ_{prompt} [%]	$\Phi_{delayed}$ [%]	Φ_{ISC} [%]	Φ_{RISC} [%]	k_F [$\times 10^6$ s^{-1}]	k_{IC} [$\times 10^6$ s^{-1}]	k_{ISC} [$\times 10^6$ s^{-1}]	k_{RISC} [$\times 10^5$ s^{-1}]
DMF-BP-DMAC	31.9	29.7	4.9	66	11	20.9	65.6	31.9	3.7	7.9	22.1	5.9
DPF-BP-DMAC	62.3	20.9	7.8	63	23	39.3	63.1	62.3	11	6.7	30.2	3.5

[a] Abbreviations: Φ_{PL} = absolute photoluminescence quantum yield; τ_{prompt} and $\tau_{delayed}$ = lifetimes calculated from the prompt and delayed fluorescence decay, respectively; $R_{delayed}$ = the ratio of delayed components; Φ_{prompt} and $\Phi_{delayed}$ = PL quantum yields of fluorescent and delayed components, respectively, determined from the total Φ_{PL} and the proportion of the integrated area of each of the components in the transient spectra to the total integrated area; Φ_{ISC} = the intersystem crossing quantum yield; k_F = fluorescence decay rate; k_{IC} = internal conversion decay rate from S_1 to S_0; k_{ISC} = intersystem crossing decay rate from S_1 to T_1; Φ_{RISC} = the reverse intersystem crossing quantum yield; k_{RISC} = the rate constant of reverse intersystem crossing process. $R_{delayed}$, Φ_{prompt}, $\Phi_{delayed}$, Φ_{ISC}, Φ_{RISC}, k_F, k_{IC}, k_{ISC} and k_{RISC} are calculated according to the equation S1-S10 in Supporting Information.

tial functions. Additionally, as temperature increases, the ratio of delayed component increases, forcefully indicating their TADF properties.

Inspired by the intriguing AIE nature, we wonder if the similar situation will occur in the aspect of delayed fluorescence. Therefore, the transient PL decay curves of DMF-BP-DMAC and DPF-BP-DMAC in solution and in neat films are depicted in Figure 4 for comparison. Both luminogens show longer lifetimes in neat films than in solutions, as illustrated in Table S2. Taking DPF-BP-DMAC as an instance, the lifetime of the delayed component in neat film ($\tau_{delayed}$ = 7.8 μs) is longer than that in solution ($\tau_{delayed}$ = 1.2 μs), which discloses its AIDF property.[15,16] The ratio of delayed components ($R_{delayed}$) and the delayed PL quantum yield ($\Phi_{delayed}$) of DPF-BP-DMAC in neat film ($R_{delayed}$ = 63% and $\Phi_{delayed}$ = 39.3%) are also higher than those in solution ($R_{delayed}$ = 31% and $\Phi_{delayed}$ = 6.8%), which corroborates the AIDF characteristic. What is more, the intersystem crossing rate constant (k_{ISC}), the rate constant of fluorescence (k_F) and the rate constant of delayed fluorescence ($k_{delayed}$) are then estimated based on the PL quantum yields and lifetime data. With regard to DMF-BP-DMAC, the results also validate its AIDF property ($\tau_{delayed}$ = 4.9 μs, $R_{delayed}$ = 66% and $\Phi_{delayed}$ = 20.9% in neat film; $\tau_{delayed}$ = 1.7 μs, $R_{delayed}$ = 27% and $\Phi_{delayed}$ = 5.9% in solution).

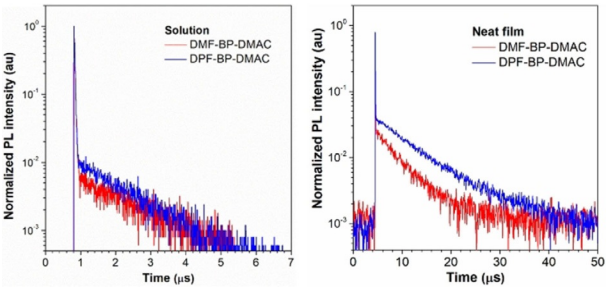

Figure 4. Transient decay PL spectra of DMF-BP-DMAC and DPF-BP-DMAC in solutions (10^{-5} mol L^{-1}) and in neat films; the data was collected at room temperature and under N_2 atmosphere.

Electrochemical behaviors

For gaining deep insights into the electrochemical behaviors of both luminogens, we investigated their experimental energy levels by cyclic voltammetry. As illustrated in Figure 5, they show reversible oxidation processes, which is an indication of their good electrochemical stability. From the Figure, it can be easily analyzed that the oxidation peaks of DMF-BP-DMAC and DPF-BP-DMAC are 1.06 eV and 1.05 eV, respectively, while the initial oxidation potentials are 0.90 eV and 0.88 eV, respectively. The energy levels of HOMOs and LUMOs are calculated to be −5.31 eV and −2.61 eV for DMF-BP-DMAC, and meanwhile, −5.29 eV and −2.51 eV for DPF-BP-DMAC, respectively, according to the methods described in Supporting Information.

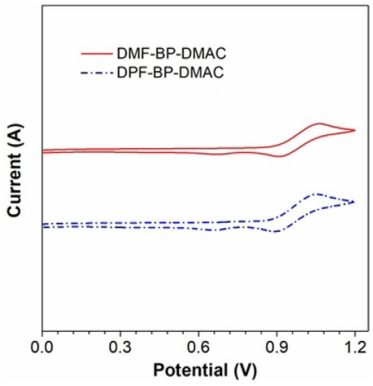

Figure 5. Cyclic voltammograms of DMF-BP-DMAC and DPF-BP-DMAC, measured in dichloromethane containing 0.1 M tetrabutylammonium hexafluorophosphate. Scan rate: 50 mV s^{-1}.

Thermal stability

To further evaluate the thermal stability of DMF-BP-DMAC and DPF-BP-DMAC, thermogravimetric analysis (TGA) and differential scanning calorimeter (DSC) are conducted. As can be seen in Figure 6, thermal decomposition temperature (T_d) and glass-transition temperature (T_g) of DMF-BP-DMAC are 322 °C and 87 °C, respectively. DPF-BP-DMAC possesses better thermal stability with higher T_d and T_g of 380 °C and 125 °C, respectively. Generally speaking, both new luminogens are suitable for OLED fabrication by thermal-deposition.

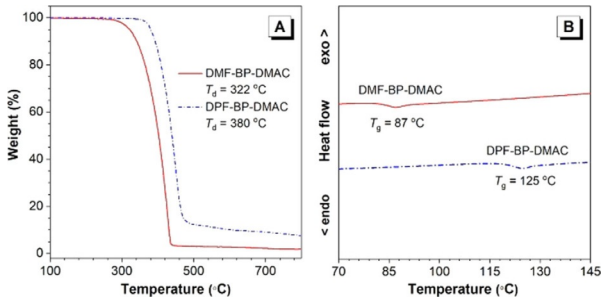

Figure 6. (A) Thermogravimetric analysis (TGA) and (B) differential scanning calorimeter (DSC) curves of DMF-BP-DMAC and DPF-BP-DMAC.

Electroluminescence

Since DMF-BP-DMAC and DPF-BP-DMAC possess prominent AIDF property and good thermal stability, it is inspiring to fabricate non-doped OLEDs based on them. One thing should be mentioned is that, to avoid triplet-energy loss, the T_1 of the adjacent layers should be higher than the luminogens. So, two types of OLED devices are carefully designed and fabricated, device I and device II (Figure 7). For device I, the configuration

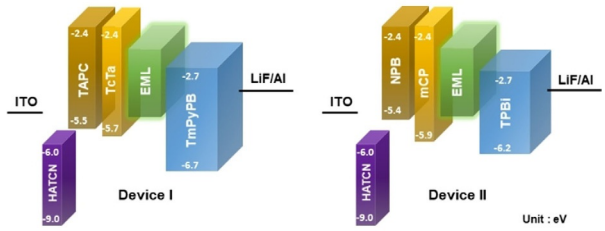

Figure 7. Configurations and energy level of non-doped OLEDs based on DMF-BP-DMAC and DPF-BP-DMAC.

is ITO/HATCN (5 nm)/TAPC (20 nm)/TcTa (5 nm)/emitter (35 nm)/TmPyPB (55 nm)/LiF (1 nm)/Al, and for device II, the configuration is ITO/HATCN (5 nm)/NPB (30 nm)/mCP (10 nm)/emitter (30 nm)/TPBi (50 nm)/LiF (1 nm)/Al. Indium-tin oxide (ITO) is a kind of transparent anode; hexaazatriphenylenehexacabonitrile (HATCN) is a commonly used hole-injection material; *N*,*N*′-bis(naphthalen-1-yl)-*N*,*N*′-bis(phenyl)benzidine (NPB) and 4,4′-cyclohexylidenebis[*N*,*N*-bis(4-methylphenyl)aniline] (TAPC) are used to transport holes in the devices; tris[4-(carbazol-9-yl)phenyl]amine (TcTa) and 9,9′-(1,3-phenylene)bis-9*H*-carbazole (*m*CP) can transport holes and block triplet excitons simultaneously since both of them have high T_1 of 2.9 eV; Neat films of DMF-BP-DMAC and DPF-BP-DMAC act as emitters in the devices; 1,3,5-tris(*N*-phenylbenzimidazol-2-yl)benzene (TPBi) and 1,3,5-tri(*m*-pyrid-3-yl-phenyl)benzene (TmPyPB) (T_1 = 2.7 eV and 2.9 eV, respectively) are utilized as electron-transporting materials and LiF/Al works as cathode. The detailed fabrication process can be seen in the Experimental Section.

The character curves are depicted in Figure 8, and key data of the devices are illustrated in Table 2. The devices are turned on at low voltages of 2.8–3.9 V and radiate stable and strong green light, owing to the proper device structures. DPF-BP-DMAC-based device I affords high maximum current efficiency, power efficiency and external quantum efficiency of 43.8 cd A^{-1}, 40.2 lm W^{-1} and 13.2%, respectively, while DMF-BP-DMAC-based device I only shows EL efficiencies of 19.9 cd A^{-1}, 16.4 lm W^{-1} and 5.7%.

The huge difference between the efficiencies of the non-doped OLEDs is probably due to the difference between neat-film Φ_{PL} values of two luminogens. The devices II afford maximum external quantum efficiencies of 6.4% and 14.4% for DMF-BP-DMAC and DPF-BP-DMAC, respectively, which are a little bit higher than those of devices I. To both DPF-BP-DMAC and DMF-BP-DMAC, the turn-on voltages of devices II are slightly higher than device I, resulting in relatively lower power efficiencies of device II. This phenomenon may be attributed to the larger hole-injection barrier of NPB/mCP interface (0.5 eV) than NPB/TcTa interface (0.2 eV). Moreover, device I of DPF-BP-DMAC retains high external quantum efficiency of 12.6% at 1000 cd m^{-2}, revealing a very small efficiency roll-off. This indicates that the high-concentration exciton annihilation at high voltages has been suppressed effectively. The highly twisted molecular conformation leads to a loose molecular packing in neat films, and thus prevents the excitons from annihilating via short-range Dexter energy transfer (DET).

To decipher the high performance of the OLEDs, the ratio of total exciton utilization is discussed. For OLEDs, the maximum external quantum efficiencies can be theoretically estimated by Equation (1),

$$\eta_{ext} = \eta_{int} \times \eta_{out} = \gamma \times \eta_{ST} \times \Phi_{PL} \times \eta_{out} \quad (1)$$

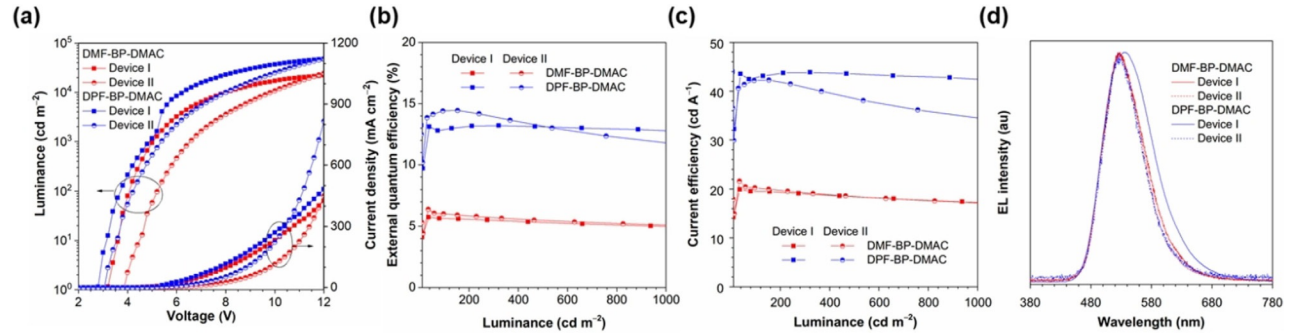

Figure 8. (a) Luminance-voltage-current density (b) external quantum efficiency-luminance, (c) current efficiency-luminance and (d) EL spectra curves of non-doped electroluminescent devices based on DMF-BP-DMAC and DPF-BP-DMAC.

Table 2. The performance of non-doped OLED devices utilizing DMF-BP-DMAC and DPF-BP-DMAC as light-emitting layers.[a]

	Device	V_{on} [V]	maximum values				values at 1000 cd m^{-2}				CIE (x,y)	λ_{EL} [nm]
			η_C [cd A^{-1}]	η_P [lm W^{-1}]	η_{ext} [%]	L [cd m^{-2}]	V [V]	η_C [cd A^{-1}]	η_P [lm W^{-1}]	η_{ext} [%]		
DMF-BP-DMAC	I	3.2	19.9	16.4	5.7	23270	5.2	16.8	10.1	4.8	(0.309, 0.595)	528
	II	3.9	21.6	14.6	6.4	32460	6.6	17.0	8.1	5.1	(0.297, 0.592)	526
DPF-BP-DMAC	I	2.8	43.8	40.2	13.2	50170	5.0	42.0	26.3	12.6	(0.346, 0.571)	534
	II	3.1	42.3	30.2	14.4	52560	5.4	34.3	19.9	11.7	(0.304, 0.560)	524

[a] Abbreviations: V_{on} = turn-on voltage at 1 cd m^{-2}; η_C, η_P, η_{ext} and L stand for current efficiency, power efficiency, external quantum efficiency and luminance for the devices, respectively. Collected at the driving voltage of 4 V, CIE and λ_{EL} represent Commission internationale de l'éclairage coordinates and the electroluminescent wavelength of each device. Device configuration: ITO/HATCN (5 nm)/TAPC (20 nm)/TcTa (5 nm)/emitter (35 nm)/TmPyPB (55 nm)/LiF (1 nm)/Al (device I); ITO/HATCN (5 nm)/NPB (30 nm)/mCP (10 nm)/emitter (30 nm)/TPBi (50 nm)/LiF (1 nm)/Al (device II).

where η_{ext}, η_{out}, γ, η_{ST} and Φ_{PL} stand for external quantum efficiency, light outcoupling efficiency (generally 0.2–0.3 without outcoupling enhancement methods), charge balance factor (ideally equal to 1), utilization ratio of electrogenerated excitons and PL efficiency of the emitting layer, respectively. Given that the DPF-BP-DMAC-based device II exhibits high η_{ext} of 14.4% and Φ_{PL} of 62.3% and assuming an ideal $\gamma = 1$ and $\eta_{out} = 0.25$, η_{ST} is calculated to be 92.7%, which is 3.7-fold of the exciton utilization limit of conventional fluorescent luminogens (25%). The result strongly indicates that neat films of DPF-BP-DMAC can efficiently harvest both singlet and triplet excitons for light emission in non-doped OLEDs owing to the intrinsic AIDF property.

Conclusions

To summarize, two D–A–D′ type luminogens, DMF-BP-DMAC and DPF-BP-DMAC, are successfully synthesized and fully characterized. They show evident AIDF properties, and can fully harvest the electrogenerated excitons in EL devices. Without the problem of concentration quenching, the non-doped OLEDs based on DPF-BP-DMAC exhibit high EL efficiencies (43.8 cd A^{-1}, 40.2 lm W^{-1} and 13.2% for device I, and 42.3 cd A^{-1}, 30.2 lm W^{-1} and 14.4% for device II), along with very small efficiency roll-off as luminance increases. With the reasonable asymmetric design strategy, a great number of AIDF luminogens with various functional substituents could be developed to further improve the efficiency and stability of non-doped OLEDs.

Experimental Section

Synthesis and Characterization

(4-Bromophenyl)(9,9-dimethylfluoren-2-yl)methanone (DMF-BP-Br): 4-Bromobenzoyl chloride (0.78 g, 3.6 mmol), 9,9-dimethylfluorene (0.58 g, 3 mmol) and 25 mL dry dichloromethane were mixed together under stirring at ambient conditions. Then anhydrous $AlCl_3$ (0.48 g, 3.6 mmol) was added into the mixture slowly and followed by stirring for 3 h at 40 °C. Then, the reaction was quenched by poured into 200 mL ice-HCl solution, and the aqueous layer was separated from the organic layer. Then the aquatic phase was further extracted with dichloromethane for several times. The combined organic layers were washed twice with water (extracted the aquatic phases again if needed), and then dried over anhydrous Na_2SO_4. After filtration and solvent evaporation under reduced pressure, the residue was purified by silica-gel column chromatography using dichloromethane/petroleum as eluent. DMF-BP-Br was obtained as a white solid in 87% yield. ^{1}H NMR (500 MHz, $CDCl_3$): $\delta = 7.91$ (d, $J = 1.0$ Hz, 1H), 7.82–7.68 (m, 5H), 7.67–7.63 (m, 2H), 7.50–7.46 (m, 1H), 7.43–7.36 (m, 2H), 1.52 ppm (s, 6H); ^{13}C NMR (125 MHz, $CDCl_3$): $\delta = 195.63$, 154.78, 153.83, 143.98, 137.83, 136.99, 135.82, 131.58, 131.51, 130.04, 128.70, 127.31, 127.18, 124.29, 122.88, 121.02, 119.57, 47.08, 26.96 ppm. HRMS (MALDI-TOF): m/z [M^+] calcd $C_{22}H_{17}BrO$, 376.0463; found, 376.0608.

(4-Bromophenyl)(9,9-diphenylfluoren-2-yl)methanone (DPF-BP-Br): The procedure was analogous to that described for DMF-BP-Br. White solid, yield 91%. ^{1}H NMR (500 MHz, [D$_6$]DMSO): $\delta = 8.15$–8.05 (m, 2H), 7.81–7.72 (m, 4H), 7.66–7.61 (m, 2H), 7.56–7.40 (m, 3H), 7.34–7.22 (m, 6H), 7.17–7.09 ppm (m, 4H); ^{13}C NMR (125 MHz, $CDCl_3$): $\delta = 195.05$, 152.20, 151.43, 145.14, 144.79, 138.78, 136.56, 136.10, 131.59, 131.48, 130.17, 129.12, 128.39, 128.17, 128.03, 127.86, 127.30, 126.97, 126.51, 121.21, 120.03, 65.57 ppm. HRMS (MALDI-TOF): m/z [M^+] calcd $C_{32}H_{21}BrO$, 500.0776; found, 500.1129.

(9,9-Dimethyl-9*H*-fluoren-2-yl)(4-(9,9-dimethylacridin-10-yl)phenyl)methanone (DMF-BP-DMAC): A mixture of DMF-BP-Br (0.74 g, 2 mmol), 9,9-dimethyl-9,10-dihydroacridine (1.00 g, 4.8 mmol), *t*BuONa (0.46 g, 6 mmol), P(*t*Bu)$_3$ (0.4 mL, 0.08 mmol), Pd(OAc)$_2$ (10 mg, 0.04 mmol) were dissolved in toluene (80 mL). The mixture was stirred and refluxed at 120 °C for 12 h under nitrogen atmosphere. After cooling to room temperature, the reaction mixture was poured into water and extracted with dichloromethane for three times. The combined organic layers were washed with water, and dried over anhydrous Na_2SO_4. After filtration and solvent evaporation, the residue was purified by silica-gel column chromatography using dichloromethane/petroleum ether as an eluent. The product was obtained as a yellow solid in 82% yield. ^{1}H NMR (500 MHz, [D$_6$]DMSO): $\delta = 8.12$–8.02 (m, 4H), 8.01–7.95 (m, 1H), 7.85 (dd, $J = 7.9$, 1.5 Hz, 1H), 7.67–7.63 (m, 1H), 7.60–7.56 (m, 2H), 7.53 (dd, $J = 7.8$, 1.4 Hz, 2H), 7.46–7.40 (m, 2H), 7.06–7.01 (m, 2H), 6.99–6.93 (m, 2H), 6.31 (dd, $J = 8.2$, 1.0 Hz, 2H), 1.64 (s, 6H), 1.53 ppm (s, 6H); ^{13}C NMR (125 MHz, [D$_6$]DMSO): $\delta = 195.37$, 154.99, 154.07, 144.99, 143.73, 140.46, 137.74, 137.51, 136.20, 132.95, 131.19, 130.72, 130.56, 129.28, 127.87, 127.05, 125.95, 124.27, 123.55, 121.78, 121.49, 120.49, 114.59, 47.24, 36.15, 31.54, 27.10 ppm. HRMS (MALDI-TOF): m/z [M^+] calcd $C_{37}H_{31}NO$, 505.2406; found, 505.2420.

(4-(9,9-Dimethylacridin-10-yl)phenyl)(9,9-diphenylfluoren-2-yl)-methanone (DPF-BP-DMAC): The procedure was analogous to that described for DMF-BP-DMAC. Yellow solid, yield 74%. ^{1}H NMR (500 MHz, DMSO): $\delta = 8.17$ (d, $J = 7.9$ Hz, 1H), 8.09 (d, $J = 7.4$ Hz,

1H), 7.98 (d, $J=8.3$ Hz, 2H), 7.93–7.87 (m, 2H), 7.57–7.42 (m, 7H), 7.35–7.22 (m, 6H), 7.20–7.14 (m, 4H), 7.06–6.91 (m, 4H), 6.28–6.23 (m, 2H), 1.63 ppm (s, 6H); ^{13}C NMR (125 MHz, [D$_6$]DMSO): $\delta=$ 195.04, 152.11, 151.32, 145.40, 145.02, 144.65, 140.41, 138.80, 137.27, 136.48, 132.93, 131.09, 130.99, 130.67, 129.81, 129.06, 128.61, 128.07, 127.49, 127.03, 126.78, 126.00, 122.26, 121.49, 121.06, 114.52, 65.53, 36.13, 31.63 ppm. HRMS (MALDI-TOF): *m/z* [M^+] calcd $C_{47}H_{35}NO$, 629.2179; found, 629.2284.

X-Ray Crystallography

Crystal data for DMF-BP-DMAC (CCDC 1572678): $C_{37}H_{31}NO$, $M_W=$ 505.63, orthorhombic, *Pbca*, $a=13.8892(10)$, $b=11.2687(7)$, $c=$ 34.863(3) Å, $V=5456.5(7)$ Å^3, $Z=8$, $\rho_{cald}=1.231$ g cm^{-3}, $\mu=$ 0.073 mm^{-1} ($Mo_{K\alpha}$, $\lambda=0.71073$), $F(000)=2144$, $T=173(2)$ K, 20459 measured reflections, 4935 independent reflections ($R_{int}=0.0760$), GOF on $F^2=1.059$, $R1=0.1047$, $wR2=0.1120$ (all data).

Crystal data for DPF-BP-DMAC (CCDC 1572671): $C_{47}H_{35}NO$, $M_W=$ 629.76, triclinic, *P-1*, $a=12.1192(9)$, $b=12.4238(8)$, $c=$ 12.7634(11) Å, $\alpha=65.698(2)^\circ$, $\beta=72.986(3)^\circ$, $\gamma=78.346(2)^\circ$, $V=$ 1667.4(2) Å^3, $Z=2$, $\rho_{cald}=1.254$ g cm^{-3}, $\mu=0.074$ mm^{-1} ($Mo_{K\alpha}$, $\lambda=$ 0.71073), $F(000)=664$, $T=173(2)$ K, 16508 measured reflections, 6052 independent reflections ($R_{int}=0.0922$), GOF on $F^2=1.030$, $R1=0.1302$, $wR2=0.1290$ (all data).

CCDC 1572671 and 1572678 contain the supplementary crystallographic data for this paper. These data can be obtained free of charge from The Cambridge Crystallographic Data Centre.

Fabrication and Characterization of OLEDs

At the very beginning of the experiment, glass substrates precoated with a 90 nm indium tin oxide (ITO) with a sheet resistance of 15–20 Ω per square were thoroughly cleaned in ultrasonic bath of detergent and deionized water, respectively, taking 30 minutes for each step. Then, the substrates were totally dried in a 65 °C oven. After that, in order to improving the hole injection ability of ITO, the substrates were treated by O_2 plasma for 10 minutes. The vacuum-deposited OLEDs were fabricated under a pressure of $<5\times10^{-4}$ Pa. Organic materials, LiF and Al were deposited at rates of 1–2 A s^{-1}, 0.1 A s^{-1}and 10 A s^{-1}, respectively.

The current density-voltage-luminance and external quantum efficiency of the devices were characterized by a dual-channel Keithley 2614B source meter and a PIN-25D silicon photodiode. The EL spectra of the devices were obtained in normal direction utilizing a spectrometer (Ocean Optics USB 2000), according to the method reported by S. R. Forrest.[17] The effective emitting area of the devices was 4 mm^2. All the characterizations were conducted at room temperature in ambient conditions without any encapsulation, as soon as the devices were fabricated.

Acknowledgements

This work was financially supported by the National Natural Science Foundation of China (21788102 and 21673082), the National Basic Research Program of China (973 Program, 2015CB655004) founded by MOST, the Guangdong Natural Science Funds for Distinguished Young Scholar (2014A030306035), the Natural Science Foundation of Guangdong Province (2016A030312002), the Science and Technology Project of Guangdong Province (2016B090907001), the Science and Technology Program of Guangzhou (201804020027), International Science and Technology Cooperation Program of Guangzhou (201704030069), and the Innovation and Technology Commission of Hong Kong (ITC-CNERC14SC01).

Conflict of interest

The authors declare no conflict of interest.

Keywords: aggregation-induced emission · excitons · fluorescence · luminescence · organic light-emitting diodes

[1] H. Sasabe, J. Kido, *J. Mater. Chem. C* **2013**, *1*, 1699–1707.
[2] a) I. Hamilton, N. Chander, N. J. Cheethan, M. Suh, M. Dyson, X. Wang, P. N. Stavrinou, M. Cass, D. C. Bradley, J.-S. Kim, *ACS Appl. Mater. Interfaces* **2018**, *10*, 11070–11082; b) L. Chen, G. Lin, H. Peng, S. Ding, W. Luo, R. Hu, S. Chen, F. Huang, A. Qin, Z. Zhao, B. Z. Tang, *Mater. Chem. Front.* **2017**, *1*, 176–180; c) L. Chen, Y. Jiang, H. Nie, P. Lu, H. H. Y. Sung, I. D. Williams, H. S. Kwok, F. Huang, A. Qin, Z. Zhao, B. Z. Tang, *Adv. Funct. Mater.* **2014**, *24*, 3621–3630; d) Y. Liu, S. Chen, J. W. Y. Lam, P. Lu, R. T. K. Kwok, F. Mahtab, H. S. Kwok, B. Z. Tang, *Chem. Mater.* **2011**, *23*, 2536–2544.
[3] a) K. Udagawa, H. Sasabe, C. Cai, J, Kido, *Adv. Mater.* **2014**, *26*, 5062–5066; b) H.-H. Kuo, Z.-I. Zhu, C.-S. Lee, Y.-K. Chen, S.-H. Liu, P.-T. Chou, A. K. Y. Jen, Y. Chi, *Adv. Sci.* **2018**, *5*, 1800846; c) T. Zhang, C. Shi, C. Zhao, Z. Wu, J. Chen, Z. Xie, D. Ma, *ACS Appl. Mater. Interfaces* **2018**, *10*, 8148–8154; d) Q. Wang, I. W. H. Oswald, X. Yang, G. Zhou, H. Jia, Q. Qiao, Y. Chen, J. Hoshikawa-Halbert, B. E. Gnade, *Adv. Mater.* **2014**, *26*, 8107–8113.
[4] D. Di, L. Yang, J. M. Richter, L. Meraldi, R. M. Altamimi, A. Y. Alyamani, D. Credgington, K. P. Musselman, J. L. MacManus-Driscoll, R. H. Friend, *Adv. Mater.* **2017**, *29*, 1605987.
[5] R. Nagata, H. Nakanotani, W. J. Potscavage, Jr., C. Adachi, *Adv. Mater.* **2018**, *30*, 1801484.
[6] a) L. Yao, B. Yang, Y. Ma, *Sci. China Chem.* **2014**, *57*, 335–345; b) W. Li, Y. Pan, R. Xiao, Q. Peng, S. Zhang, D. Ma, F. Li, F. Shen, Y. Wang, B. Yang, Y. Ma, *Adv. Funct. Mater.* **2014**, *24*, 1609–1614.
[7] a) C. Adachi, *Jpn. J. Appl. Phys.* **2014**, *53*, 060101; b) Y. Tao, K. Yuan, T. Chen, P. Xu, H. Li, R. Chen, C. Zheng, L. Zhang, W. Huang, *Adv. Mater.* **2014**, *26*, 7931–7958; c) T. Huang, W. Jiang, L. Duan, *J. Mater. Chem. C* **2018**, *6*, 5577–5596; d) X. Cai, S.-J. Su, *Adv. Funct. Mater.* **2018**, 1802558; e) Q. Zhang, D. Tsang, H. Kuwabara, Y. Hatae, B. Li, T. Takahashi, S. Y. Lee, T. Yasuda, C. Adachi, *Adv. Mater.* **2015**, *27*, 2096–2100; f) T. A. Lin, T. Chatterjee, W. L. Tsai, W. K. Lee, M. J. Wu, M. Jiao, K. C. Pan, C. L. Yi, C. L. Chung, K. T. Wong, C. C. Wu, *Adv. Mater.* **2016**, *28*, 6976–6983.
[8] a) P. Rajamalli, N. Senthilkumar, P. Gandeepan, P.-Y. Huang, M.-J. Huang, C.-Z. Ren-Wu, C.-Y. Yang, M.-J. Chiu, L.-K. Chu, H.-W. Lin, C.-H. Cheng, *J. Am. Chem. Soc.* **2016**, *138*, 628–634; b) P. Rajamalli, N. Senthilkumar, P.-Y. Huang, C.-C. Ren-Wu, H.-W. Lin, C.-H. Cheng, *J. Am. Chem. Soc.* **2017**, *139*, 10948–10951; c) G. Xie, J. Luo, M. Huang, T. Chen, K. Wu, S. Gong, C. Yang, *Adv. Mater.* **2017**, *29*, 1604223; d) X. Cai, X. Li, G. Xie, Z. He, K. Gao, K. Liu, D. Chen, Y. Cao, S.-J. Su, *Chem. Sci.* **2016**, *7*, 4264–4275.
[9] a) D. Zhang, P. Wei, D. Zhang, L. Duan, *ACS Appl. Mater. Interfaces* **2017**, *9*, 19040–19047; b) F. B. Dias, J. Santos, D. R. Graves, P. Data, R. S. Nobuyasu, M. A. Fox, A. S. Batsanov, T. Palmeira, M. N. Berberan-Santos, M. R. Bryce, A. P. Monkman, *Adv. Sci.* **2016**, *3*, 1600080; c) P. L. dos Santos, J. S. Ward, M. R. Bryce, A. P. Monkman, *J. Phys. Chem. Lett.* **2016**, *7*, 3341–3346; d) J.-A. Seo, Y. Im, S. H. Han, C. W. Lee, J. Y. Lee, *ACS Appl. Mater. Interfaces* **2017**, *9*, 37864–37872; e) C. Li, R. Duan, B. Liang, G. Han, S. Wang, K. Ye, Y. Liu, Y. Yi, Y. Wang, *Angew. Chem. Int. Ed.* **2017**, *56*, 11525–11529; *Angew. Chem.* **2017**, *129*, 11683–11687; f) Y. Yuan, Y. Hu, Y.-X. Zhang, J.-D. Lin, Y.-K. Wang, Z.-Q. Jiang, L.-S. Liao, S.-T. Lee, *Adv. Funct. Mater.* **2017**, *27*, 1700986.
[10] C. Murawski, K. Leo, M. C. Gather, *Adv. Mater.* **2013**, *25*, 6801–6827.
[11] Y. Zaushitsyn, K. G. Jespersen, L. Valkunas, V. Sundström, A. Yartsev, *Phys. Rev. B* **2007**, *75*, 125328.
[12] D. Song, S. Zhao, Y. Luo, H. Aziz, *Appl. Phys. Lett.* **2010**, *97*, 243304.

[13] S. Reineke, K. Walzer, K. Leo, *Phys. Rev. B* **2007**, *75*, 123528.
[14] a) L. Chen, Y. Jiang, H. Nie, R. Hu, H. S. Kwok, F. Huang, A. Qin, Z. Zhao, B. Z. Tang, *ACS Appl. Mater. Interfaces* **2014**, *6*, 17215 – 17225; b) G. Lin, H. Peng, L. Chen, H. Nie, W. Luo, Y. Li, S. Chen, R. Hu, A. Qin, Z. Zhao, B. Z. Tang, *ACS Appl. Mater. Interfaces* **2016**, *8*, 16799 – 16808; c) H. Nie, B. Chen, J. Zeng, Y. Xiong, Z. Zhao, B. Z. Tang, *J. Mater. Chem. C* **2018**, *6*, 3690 – 3698; d) B. Chen, B. Liu, J. Zeng, H. Nie, Y. Xiong, J. Zou, H. Ning, Z. Wang, Z. Zhao, B. Z. Tang, *Adv. Funct. Mater.* **2018**, *28*, 1803369.
[15] a) J. Guo, J. Fan, L. Lin, J. Zeng, H. Liu, C.-K. Wang, Z. Zhao, B. Z. Tang, *Adv. Sci.* **2018**, 1801629; b) J. Guo, Z. Zhao, B. Z. Tang, *Adv. Opt. Mater.* **2018**, *6*, 1800264; c) H. Liu, J. Zeng, J. Guo, H. Nie, Z. Zhao, B. Z. Tang, *Angew. Chem. Int. Ed.* **2018**, *57*, 9290 – 9294; *Angew. Chem.* **2018**, *130*, 9434 – 9438; d) J. Huang, H. Nie, J. Zeng, Z. Zhuang, S. Gan, Y. Cai, J. Guo, Z. Zhao, B. Z. Tang, *Angew. Chem. Int. Ed.* **2017**, *56*, 12971 – 12976; *Angew. Chem.* **2017**, *129*, 13151 – 13156; e) J. Guo, X.-L. Li, H. Nie, W. Luo, S. Gan, S. Hu, R. Hu, A. Qin, Z. Zhao, S.-J. Su, B. Z. Tang, *Adv. Funct. Mater.* **2017**, *27*, 1606458; f) J. Guo, X.-L. Li, H. Nie, W. Luo, R. Hu, A. Qin, Z. Zhao, S.-J. Su, B. Z. Tang, *Chem. Mater.* **2017**, *29*, 3623 – 3631; g) S. Gan, J. Zhou, T. A. Smith, H. Su, W. Luo, Y. Hong, Z. Zhao, B. Z. Tang, *Mater. Chem. Front.* **2017**, *1*, 2554 – 2558.
[16] a) L. Yu, Z. Wu, G. Xie, W. Zeng, D. Ma, C. Yang, *Chem. Sci.* **2018**, *9*, 1385 – 1391; b) L. Yu, Z. Wu, G. Xie, C. Zhong, Z. Zhu, D. Ma, C. Yang, *Chem. Commun.* **2018**, *54*, 1379 – 1382; c) F. Ni, Z. Zhu, X. Tong, M. Xie, Q. Zhao, C. Zhong, Y. Zou, C. Yang, *Chem. Sci.* **2018**, *9*, 6150 – 6155.
[17] S. R. Forrest, D. D. C. Bradley, M. E. Thompson, *Adv. Mater.* **2003**, *15*, 1043 – 1048.

Manuscript received: October 29, 2018
Accepted manuscript online: November 25, 2018
Version of record online: December 10, 2018